

Sample Acquisition and In-Situ Analysis Using the Ultrasonic/Sonic Driller/Corer (USDC) and Robotic Platforms

Stewart Sherrit, Yoseph Bar-Cohen, Benjamin P. Dolgin, Nathan Bridges, Xiaoqi Bao, Zensheu Chang, Albert Yen, Ronald S. Saunders, Richard A. Rainen, Stephen F. Dawson JPL/Caltech, (MS 82-105), 4800 Oak Grove Drive, Pasadena, CA 91109-8099, yosi@jpl.nasa.gov, web: <http://ndeaa.jpl.nasa.gov>
Dharmendra Pal, Jason Kroh, Tom Peterson
Cybersonics Inc., Erie, PA

Abstract – Future NASA exploration missions to Mars, Europa, Titan, comets and asteroids are seeking to perform sampling, in-situ analysis and possibly return of material to Earth for further tests. One of the major limitations of sampling in low gravity environments is the conventional drills need for high axial force and, as a result, heavy robotic mechanisms are required which constrain mission objectives. To overcome this and other limitations of existing drilling techniques, an ultrasonic/sonic driller/corer (USDC) mechanism was developed. The USDC is based on an ultrasonic horn that is driven by a piezoelectric stack. The horn drives a free mass, which resonates, between the horn and drill stem. Tests have shown that this device addresses some of the key challenges to the NASA objective of planetary in-situ sampling and analysis. The USDC is lightweight (450 g), requires low preload ($< 5\text{N}$) and can be driven at low power (5W). The device has been operated from a Sojourner class rover and the FIDO robotic arm. In addition the device has been shown to drill various rock types including granite, diorite, basalt and limestone. The drill has the potential to be operated at high and low temperatures and does not require sharpening of the bit. Although the drill is driven electrically at 20 kHz, a substantial sub-harmonic acoustic component is found that is crucial to drilling performance. Analytical models that explain this low frequency coupling in the horn, free mass, drill stem and rock were developed and are currently being integrated and verified. The results of the USDC research and development efforts so far and the potential of the device will be describe in this paper.

1. INTRODUCTION

The performance of efficient drilling and coring of rock materials has a great significance to the NASA planetary program. In general a sample needs to be cored, analyzed and possibly returned to earth. Other fields that may also benefit from of an effective sampling technologies include; the military, medical operations, construction, geology, sports (e.g., hiking), and games. Existing drilling techniques are limited by the need for large axial forces, high power

consumption, and heavy mechanisms. Other areas of concern associated with conventional drilling technologies are that they are subject to bit jamming, breaking, dulling and are difficult to use to perform non-vertical drilling. In addition the life of standard coring bits is markedly reduced by the breakdown of the binder that holds the abrasive material on the bit surface.

The ability of the new ultrasonic/sonic driller/corer (USDC) to operate with minimum axial load (see Figure 1) is offering important enabling tools for sample acquisition and analysis. Current research and development efforts of the authors are dedicated to understanding the drilling mechanism as well as analytically modeling its operation towards the goal of optimizing device performance in various configurations.

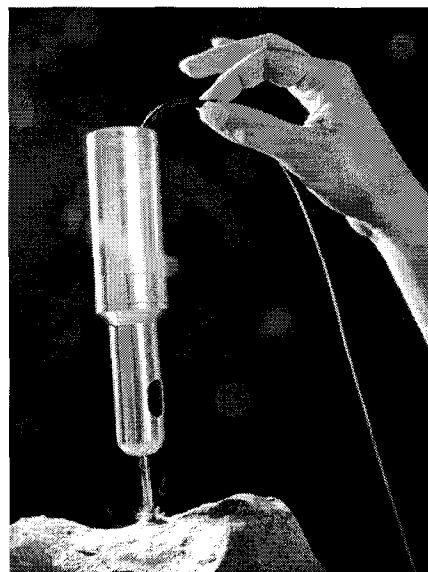


Figure 1 – A photographic view of the USDC held from its cable while coring sandstone. The minimal need for axial force is easily seen.

The device consists of three main parts; an ultrasonic actuator consisting of a piezoelectric stack and horn, a free mass and a drill stem. The analysis of the actuator circuit was based on the equivalent circuit of piezoelectric and acoustic

elements as discussed by Mason [1], [2] and was reported

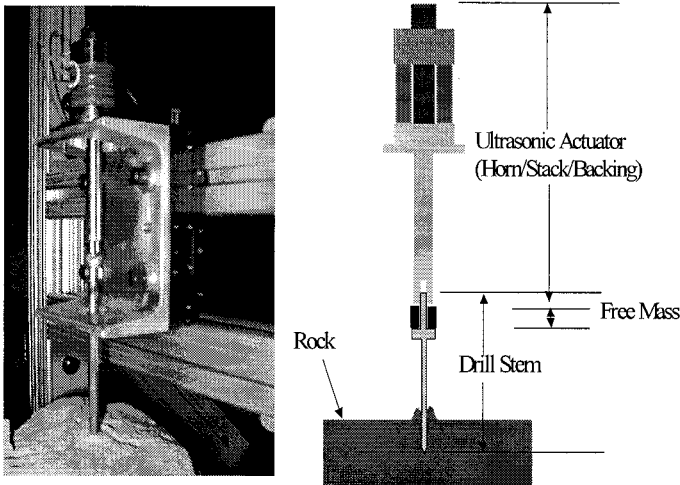


Figure 2 - Photograph and Schematic of the Ultrasonic/Sonic Driller/Corer, which is mounted on a test rig in the photograph.

previously [3], [4]. The standard horn was found to have a resonance at 21.5 kHz and the free tip velocity at resonance was determined to be linear with respect to the applied voltage and ranged from 1 to 10 m/s depending on the acoustic load as is shown in Figure 3.

The vibrations of the horn tip excite the free mass, which resonates between the horn tip and the top of the drill stem at frequency of the order of 1000 Hz. Acoustic energy in the free mass resonator is transferred to the top of the drill stem and propagates to the bit/rock interface where the rock is excited past its ultimate strain and fractures. In order to determine the critical issues related to the control and optimization of the drill initial modeling of the acoustic interaction at the various interfaces of the drill was investigated. The three interfaces that were studied are: 1) the interaction of the horn tip with the free mass, 2) the interaction of the free mass with the drill stem and 3) the interaction of the base of the drill stem (bit) with the rock.

2. MODELING

In order to proceed with the modeling the velocity/displacement of the horn tip during operation is required. Since the velocity/displacement depends on the acoustic load a reasonable estimate of the velocity range can be determined by calculating the horn tip velocity for the case where it is free and when the acoustic impedance is perfectly matched to produce maximum power in the acoustic load. The velocity of the tip as a function of the applied peak AC voltage is shown in Figure 3 for the two cases. The reasons for using the case where the acoustic load is ideal rather than clamped are twofold. Firstly the acoustic power transferred to the rock is substantial which means that horn is well matched to the rest

of the acoustic elements and secondly in order for the device to operate efficiently a gap must be present which means that for a substantial portion of the time the tip is not in contact with the free mass. For a peak AC voltage of 200 Volts on the drill the velocity is found to range between 1.25 m/s for the ideal load and 13.6 m/s for the free tip. The modeling of the interaction of the free mass can now be determined since the range of speeds of the horn tip have been set.

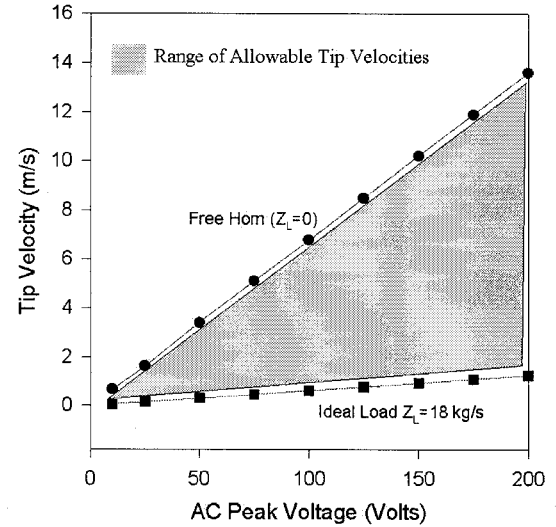


Figure 3 - The range of speed for the horn tip for an ideal load and for the unloaded horn.

Horn Tip – Free Mass Interaction

The free mass is driven by the horn tip, which vibrates at resonance frequency. A schematic of the model is shown in Figure 4. The tip displacement is harmonic and is describe by

$$u = u_0 \cos(\omega t + \theta). \quad (1)$$

The velocity of the horn tip is found by taking the time derivative of the displacement and is

$$v = -\omega u_0 \sin(\omega t + \theta). \quad (2)$$

Assuming the energy loss and time duration of the impact is negligible and the mass of the horn is much larger than

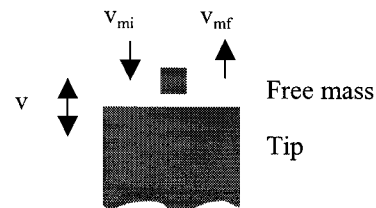


Figure 4 - A schematic of the free mass horn tip interaction model.

the free mass, we find using conservation of momentum and energy that

$$v_{mf} = v_{mi} + 2v \quad (3)$$

where v_{mi} is the free-mass velocity prior to interaction with horn and v_{mf} is the free mass velocity after interaction with the horn. A computer simulation model that traces the positions of the free mass until it leaves the tip vibration range ($2u_0$) was written. The routine calculates the free mass speed after interaction with the horn. By keeping track of the free mass velocity the routine allowed us to explore this driving mechanism as a function of the horn position as the free mass crosses the plane of full extension (phase). The speed of the free mass as it leaves the interaction region versus position of the horn (position of tip represented as a phase angle $t=0$ at max displacement) was calculated for various ratios of v_{mi}/v .

For all cases there is a net increase in the free mass velocity after interaction with the horn when averaged over phase. The computer model traces the movements of the free-mass and the horn. The movement of the horn is due to the reaction force on the horn tip and the force of gravity. In the calculation the free mass is set to 1 gram, the tip velocity amplitude is set to 1.26 m/s corresponding to displacement amplitude of 10 μ m. The horn mass was 800 g (including mass of test-rig). The energy loss of the free mass in each round trip is set as 75%. The ratio of the free mass velocity to the maximum horn tip velocity as a function of time was simulated and the results were used to calculate the motion of the horn. The results show the random characteristics of the movement of the body of the horn. Figure 5 shows the calculated horn tip position as a function of time. The motion is due to the impact interaction with the free mass.

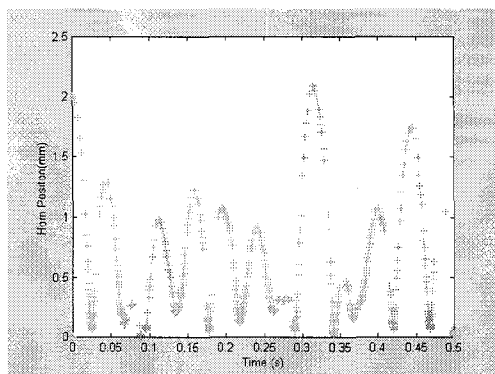


Figure 5 - The horn position calculated as a function of time determined from model.

The size, frequency and randomness of the jumps are confirmed by experimental observations shown in Figure 6 of the horn tip determined using a high-speed camera.

Free mass, Drill stem Interaction

The free mass impacts the top of the drill stem and creates a stress wave that propagates to the bit end. A finite element model was utilized to investigate the impact and resultant stress wave. Figure 7 shows results for the case where a

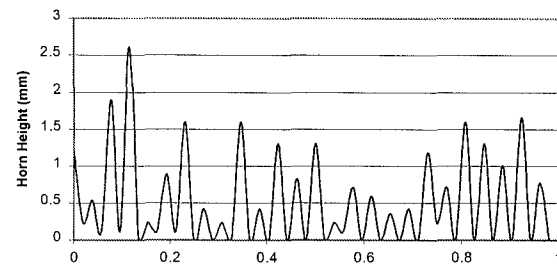


Figure 6 - The horn position as a function of time determined from high-speed camera.

cylindrical steel stem/bit of diameter 3.0 mm and length 100 mm with a concentric top cap of diameter 12 mm and length 6 mm. The impact used in the model is that of a free mass of 2 g with speed 1 m/s. The free mass has a curved surface at the contact area with a curvature of 10 mm. The free mass is assumed to be rigid and the bit end of the drill stem is clamped. Figure 7 shows the displacement of the surface of the free mass and the top surface of the drill stem during impact as a function of time. Figure 8 shows the resultant stress wave as a function of time at the bit end of the drill stem.

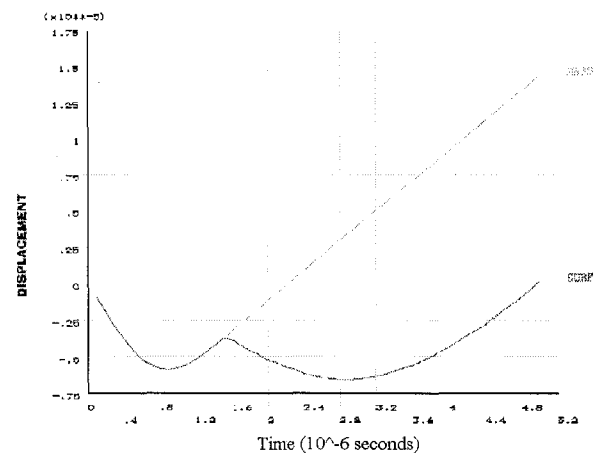


Figure 7 - The displacement as a function of time of the free mass and the top surface of the drill stem after impact.

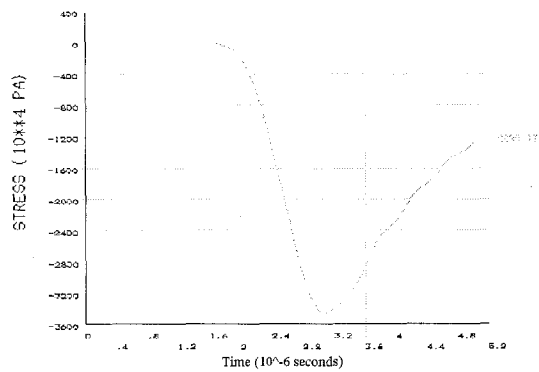


Figure 8 - The stress as a function of time of the free mass and the top surface of the drill stem after impact.

Bit Rock Interaction

In order to better understand the fracture of rocks under impact loading from a drill or a corer, a finite element model was developed using ANSYS. For the purpose of simplifying the problem, the rock is modeled as a circular cylinder with bottom surface fixed and the drill/corer impacts at the center of the top surface. This simplification makes the problem axis-symmetric. By using the axis-symmetric elements available in ANSYS, the original three-dimensional problem is now reduced to a two-dimensions. The element size is made very fine near the drill/corer bit, and becomes coarser and coarser as it goes further away from the bit. Figure 9 shows a typical mesh for the problem outlined above.

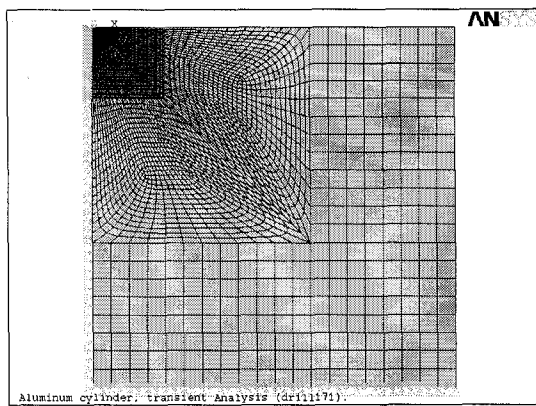


Figure 9- The mesh used to solve the bit rock interaction

Preliminary results were derived by assuming that the circular cylinder is made of isotropic material with a Young's modulus of 10 GPa and Poisson's ratio of 0.3. The impact loading from the drill has a peak value of .1 GPa and duration of 2.5 μ sec, as shown in Figure 8.

Contour maps of the maximum principal strain were plotted and used as indication of fracture of rocks. It also shows how the elastic waves propagate in the rock. Figures 10 show the contour maps for the cylinder for drilling and

coring, respectively. The drill bit is 3 mm in diameter. The corer has an inner diameter of 2 mm and an outer diameter of 3 mm.

The results show qualitative features of the rocks fracture under ultrasonic drilling or coring. From Figure 10 we find that the highest principal strain occurs at the edge of the drill bit. Also, the highest principal strain appears at both the outer and inner edge of the corer. It implies that the fracture is likely going to happen at the edge, which is confirmed by viewing the high speed filming during drilling. By comparing the various strain profiles in Figure 10, we find that the maximum principal strain under coring is higher than that under drilling, and the area of high principal strain under coring is

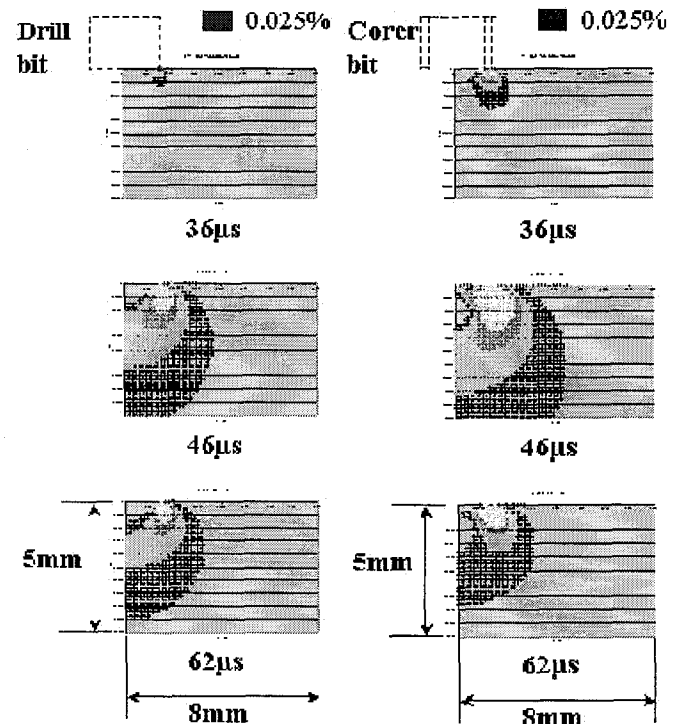


Figure 10 - The principle strain profile at various times after impact of the free mass on the drill stem for a drilling bit and a coring bit.

also larger than that under drilling. It implies that with the same outer diameter and under the same loading, a corer will drill faster than a solid drill of the same diameter. This is confirmed by experiments.

The results have show how drilling and coring can be achieved with little or no preload. The next challenge is to integrate each of the models to determine the limits and optimization of the USDC. A more complete description of the modeling of the horn/free mass/drill interaction can be found in recent publications [5], [6], [7]

3. DRILL CONFIGURATIONS

A wide variety of bit designs have been tested using the USDC as is shown in Figure 11. The bits can be separated into three main categories; drilling, coring and rock abrasion.

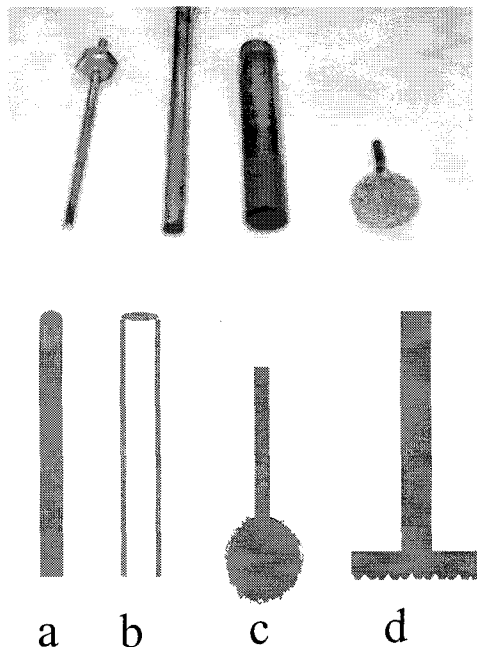


Figure 11. Schematic and photograph of some the various bits that have been designed and tested. They include tungsten carbide flat bit drills(a), stainless coring tubes (b), tungsten carbide fiber coated spheres (c) and an abrasion bit formed by a 2D array of pyramidal bits (d).

a) Drilling

In order to investigate the drill performance that would be expected when drilling on Mars a series of rocks were acquired that NASA geologists suggested would be similar in the range of mechanical properties expected of the rock types found on Mars. Drilling tests were performed on these rock samples using the USDC in the test rig shown in Figure 1. The depth as a function of time is shown in Figure 12 for a flat drill bit 2.85 mm in diameter. The tests shown were undertaken using 12-Watts average power (24-Watts peak power- 50% duty cycle). The power was measured at the input of the electronics and includes circuit loss of the driving electronics. The drill depth as a function of time can be generally be described by the functional relationship

$$D(t) = D_0 t^n \quad (4)$$

Where D_0 and n are constants that depend on the drill geometry and rock type for a given power level. The value of the constant n is between 0 and 1. The drill rate is found by taking the time derivative and is

$$R(t) = nD_0 t^{n-1} \quad (5)$$

The rate is seen to decrease as a function of the time (depth). This saturation is likely due to a combination of causes including the collection of tailings at the face of the bit damping the impact on the rock, viscous drag of the tailings on the drill stem and possibly inhomogeneity of the elastic properties of the rock.

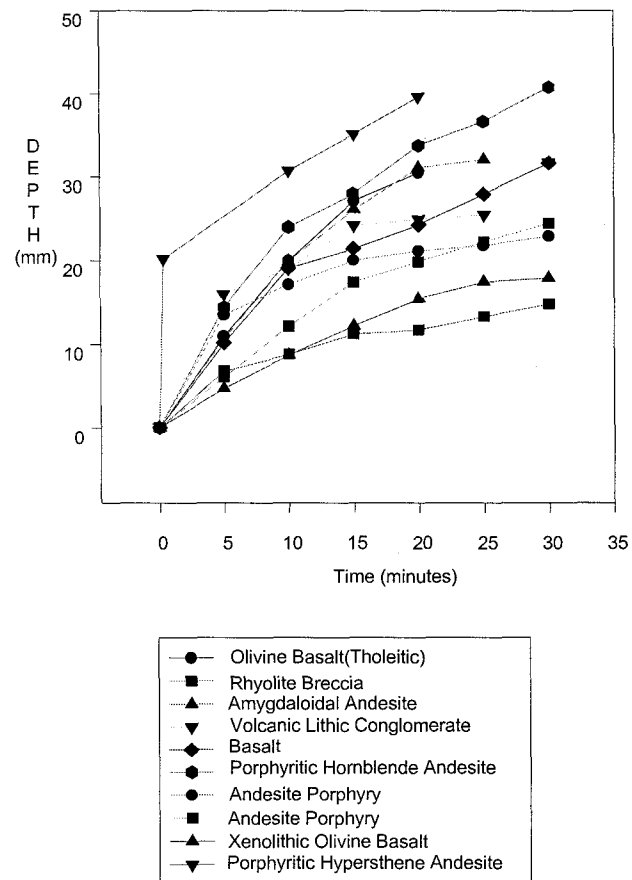


Figure 12 - The depth in mm as a function of time for various rock types (set #1)

b) Coring Tools

A variety of coring bits have been fabricated with core diameters ranging from 2mm to 10mm (Figure 11.). The penetration rates into the rock material have been found to vary to first order with the inverse of the cross sectional area of the coring bit. Core integrity has been found to depend on rock type and diameter of the coring bit. The smaller the core diameter the more likely for a core shearing fracture to propagate throughout the core area. Cores as small as 5 mm in diameter have been obtain in soft rock (Sandstone) however in harder rocks such as Basalt larger diameter corers are required to maintain the core integrity.

c) Rock Abrasion Tools

An example of rock abrasion is shown in Figure 13. The letters JPL were carved into the Basalt using the tungsten carbide coated sphere in approximately 40 minutes using 12 watts power. In order to more fully understand the geology of Mars, instrument access to un-weathered rock surfaces is of considerable importance for future missions. To this end an



Figure 13. Basalt rock sample tested using the abrasion tools shown in Figure 11.

ultrasonic rock abrasion tool (URAT) is currently being designed and tested. The device was designed to be light (<0.500 kg) consuming less than 30-Watts power while removing 5 mm of rock from a 40 mm diameter area. The abrasion tool for this device is a 40 mm diameter bit with a 2D array of pyramidal bits. An example of the abrasion for these bit designs is shown in the circular area abraded in the Basalt sample shown in Figure 13.

4. SAMPLE INTEGRITY

In order to test that the mineralogy of the rock is not altered by the drilling action four samples of drill tailings were collected from the USDC and the powder was analyzed and compared to lab ground powders of the same material. The five rock samples chosen for the study were; Iron Oxide, 2 Iron Oxyhydroxides samples, Pyroxene and a Carbonate sample. An example comparison of the absorbance and the X-ray diffraction for the lab ground powder and USDC tailings are shown in Figure 14 and 15. In general only minimal differences were present between the two powder production techniques. Further tests on the mineralogy, elemental chemistry, crystal size, and oxidation caused by local heating during drilling are required to determine the full effects if any of ultrasonic/sonic drilling on the powder and core specimens.

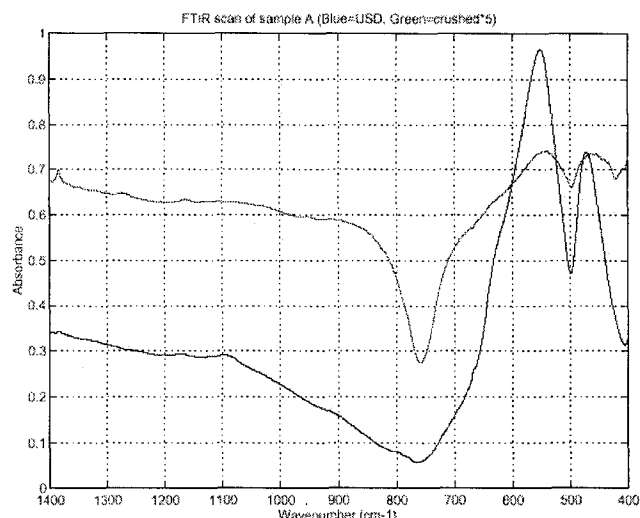


Figure 14. The FTIR spectra of the lab ground (green line) and the USDC produce powder for a hematite rock sample. Peaks in the spectra are found to overlap.

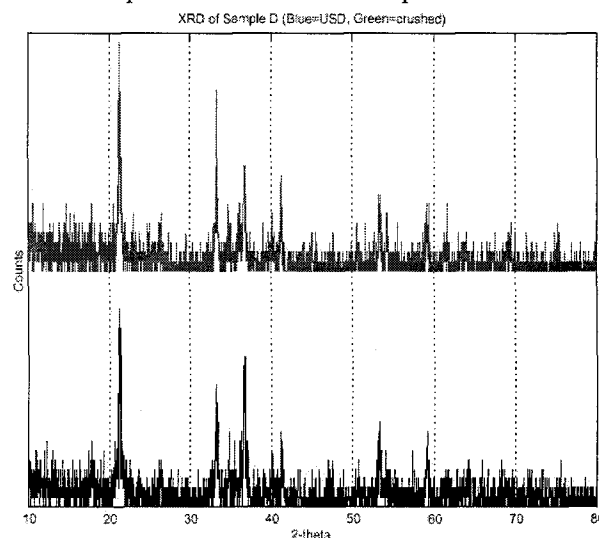


Figure 15. XRD spectra of the lab ground (green line) and the USDC produce powder for a Iron Oxyhydroxide rock sample. Peaks in the spectra are found to overlap. There is no evidence of conversion to hematite during drilling.

5. DRILLING PLATFORMS

Although the majority of tests discussed above have been performed on the test-rig shown in Figure 2. The USDC has been operated successfully from a Sojourner class rover scaled down to be the same weight on Earth as it would be on Mars (Figure 16.). Drilling and coring were performed from the rover without any mechanical interaction with the body of the rover even when axial loads applied from the rover were large enough to clamp the sonic component of the drill.

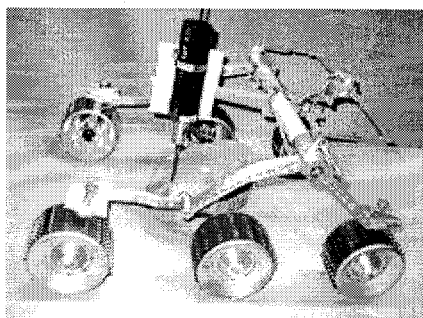


Figure 16. Coring from a Sojourner class rover.

Drilling was also demonstrated from the arm of the Field Integration Design and Operations rover (FIDO) shown in Figure 17. During the tests the USDC drilled into a limestone rock. The drill was removed from the drill-hole and the hole was re-acquired using the FIDO robotic arm.

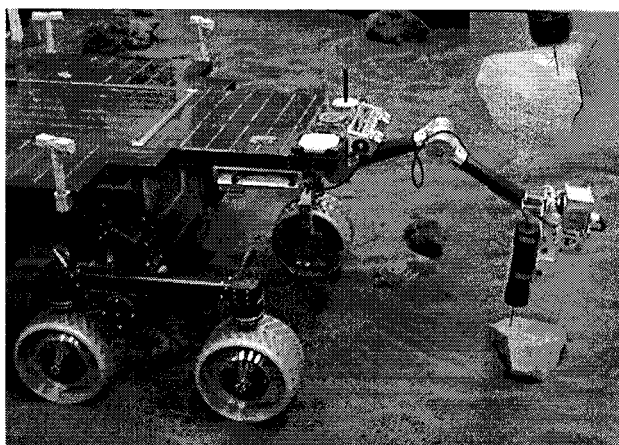


Figure 17. Drilling from the arm of the FIDO rover. The hole was reacquired after the drill and arm were stowed.

5. INTEGRATED SENSOR/SAMPLER

A recent development is the Smart USDC [8], which has integrated sensors to determine various rock properties prior to and during drilling. In addition the core, dust and any volatiles have the ability to be extracted through the device for in-situ analysis or stored for sample return. A prototype USDC and schematic diagram with the coring bit running through the actuator is shown in Figure 18. Due to the fact that the USDC operates in extension rather than rotation sensors can be embedded in the coring and drilling bits. Properties that may be determined with integrated sensors include; thermocouples, RF transducers and receivers, eddy-current devices, acoustical sensors, conductivity and dielectric properties sensors, and fiber-optic based devices (visible/IR

spectrometers, photoluminescence devices, and Raman spectrometers to name a few).

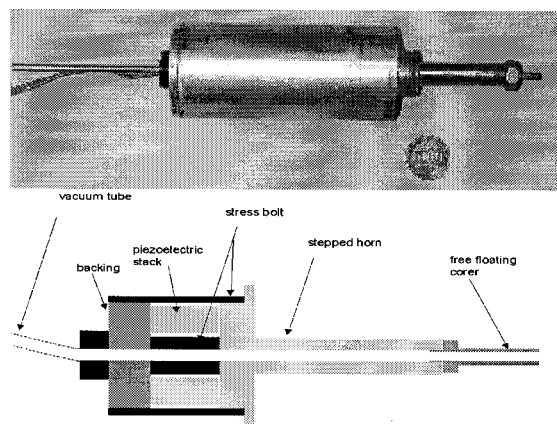


Figure 18. A prototype smart USDC with the capability for sample extraction through the actuator.

Another aspect of the smart USDC relies on the inherent acoustic properties of the device. The sonic component of the USDC can be used as a source for sonar to investigate the presence of layers. These layers cause dispersive wave characteristics, small discontinuities cause scattering and attenuation, and large discontinuities (rocks, cavities, etc.) produce reflections. Methods are available to extract geophysical information from the imparted waves, offering effective probing, imaging and providing valuable information about the stiffness constants and other mechanical properties of soil and rocks. In addition the ultrasonic component generated at the horn tip may be used to investigate the acoustic impedance of contacting samples. The horn/actuator is a high Q resonator and when the horn comes in contact with a structure it radiates ultrasonic energy into the structure, which can among other things reduce the resonance frequency and lower the quality Q of the resonance. The degree to which this occurs is a function of the acoustic impedance (product of the density and velocity of sound) in the contacting material.

6. CONCLUSIONS

A new drilling, coring and rock abrasion mechanism was reported which operates at low power and low axial force. The device was demonstrated to operate from a Sojourner class rover and the robotic arm of FIDO with very little mechanical coupling to the robotic platform. A piezoelectric stack driven at 20 kHz that is connected to an ultrasonic horn actuates the device. The interaction of the horn with the free-mass and drill stem creates substantial sub-harmonic acoustic components, which generates a significant impact force at the

rock bit interface. Analytical models were presented to explain the low frequency coupling between the horn and free mass. Current efforts are underway to integrate the various models to create a system model with predictive capabilities for the optimization of the device. Initial rock sample integrity results suggest no deleterious effects on powder samples acquired using the USDC. The concept of the smart USDC with integrated sensors for in-situ sampling and analysis was discussed

ACKNOWLEDGMENT

The authors would like to thank J.D. Carson for design and fabrication of the test apparatus. Dr. Paul Schenker and Dr. Eric Baumgartner for access to and aid in the FIDO robotic arm drilling test. The Mars Exploration Technologies under a contract with the National Aeronautics Space Agency (NASA) funded the research at the Jet Propulsion Laboratory (JPL), a division of the California Institute of Technology.

REFERENCES

- [1] W. P. Mason, Electromechanical Transducers and Wave Filters, Princeton, NJ, Van Nostrand, 1948
- [2] W.P. Mason, Physical Acoustics and the Properties of Solids, D. Van Nostrand Co., Princeton, NJ, 1958
- [3] S. Sherrit, B.P. Dolgin, Y. Bar-Cohen, D. Pal, J. Kroh, T. Peterson "Modeling of Horns for Sonic/Ultrasonic Applications," Proceedings of the IEEE International Ultrasonics Symposium, Lake Tahoe, CA, October 1999, pp. 647-651
- [4] Y. Bar-Cohen, S. Sherrit, B. P. Dolgin, D. Pal, T. Peterson, J. Kroh, R. Krahe, "Ultrasonic/sonic drilling/coring (USDC) for in-situ planetary applications," SPIE Smart Structures 2000, March 2000, Newport Beach, CA, paper 3992-101
- [5] S. Sherrit, X. Bao, Z. Chang, B.P. Dolgin, Y. Bar-Cohen, D. Pal, J. Kroh, T. Peterson, "Modeling of the Ultrasonic/Sonic Driller/Corer: USDC," Proceedings of the IEEE Ultrasonics Symposium in San Juan, Puerto Rico, pp. 691-694, Oct 22-25, 2000
- [6] Y. Bar-Cohen, S. Sherrit, B.P. Dolgin, X. Bao, Z. Chang, D. Pal, R. Krahe, J. Kroh, S. Du, T. Peterson "Ultrasonic/sonic drilling/coring (USDC) for planetary applications," SPIE Smart Structures 2001, March 2001, Newport Beach, CA, paper 4327-55
- [7] Xiaqi Bao, Zensheu Chang, Stewart Sherrit, Benjamin P. Dolgin, Yoseph Bar-Cohen, Dharmendra S. Pal, Shu Du, Thomas Peterson, "Modeling and Computer Simulation of Ultrasonic/Sonic Driller/Corer (USDC)" To be published - In preparation
- [8] Y. Bar-Cohen, S. Sherrit, B. Dolgin, T. Peterson, D. Pal and J. Kroh, "Ultrasonic/Sonic Driller/Corer (USDC) With Integrated Sensors," New Technology Report, Submitted on August 30, 1999. Docket No. 20856, Item No. 0448b, November 17, 1999, Provisional Patent, filed on May 3, 2000, Application No. 60/201,650. Currently, a patent is being filed